Master's Thesis

Near-infrared fluorophores and cyclodextrin complex for improved cancer imaging and phototherapy

Department of Biomedical Sciences
Graduate School, Chonnam National University

Bo Young Lee

August 2022

CONTENTS

Near-infrared fluorophores and cyclodextrin complex for improved cancer imaging and phototherapy

Bo Young Lee

Department of Biomedical Sciences,
Chonnam National University Medical School, Gwangju, South Korea
(Supervised by Professor Hoon Hyun)

Abstract

Near-infrared (NIR) fluorescence cancer imaging with aimed NIR fluorophores can potentially be used to detect and diagnose cancer. IR783, as a singular molecule, has been extensively utilized for tumor imaging without the addition of moieties. Therefore, this approach is efficient in combination with various carbocyanine dyes to enhance tumor imaging. A biocompatible supramolecular complex self-built from methyl-β-cyclodextrin (Mβ-CD) and indocyanine green (ICG) was generated to address cancer imaging, and further upgrade fluorescence-guided photothermal cancer therapy. This study approved that the development of a composition of complex compounds Mβ-CD and ICG inner cavity could lead to an enhanced tumor imaging in contrast to free ICG. The complex compound ICG-CD could be utilized as a bifunctional phototherapeutic agent to address cancer phototherapy as a result of the high tumor focus Mβ-CD moiety and the efficacious performance of the

NIR ICG moiety. The photothermal outcome exerted by the heterocyclic complex ICG-CD upon NIR laser irradiation remarkably boosted the temperature at the site of the tumor by 56.2℃ within 5 minutes. Using the ICG-CD complex in targeting HT-29 tumors in 9-days photothermal treatment resulted in a clear reduction in tumor volumes.

Additionally, no body weight loss or tumor recurrence was observed after administering the ICG-CD complex alongside NIR laser irradiation.

Therefore, the biocompatible complex, ICG-CD, and NIR laser treatment can be used in the future for clinical purposes as a potential strategy for tumor targeting.

1. Introduction

Cancer phototherapy in combination with a phototheranostic drug has piqued the interest of researchers around the globe, owing to the possibility of increasing therapeutic outcomes through the use of this technique [1-3]. Biocompatibility, tumor specificity, imaging ability, along with phototherapeutic ability are among the most significant properties of an excellent phototheranostic drug [4-8]. Indocyanine green (ICG) is a therapeutically accessible near-infrared (NIR) fluorophore that performs various functions such as a photosensitizer, photothermal agent, as well as a fluorescence imaging probe [9-11]. It is one of numerous phototherapeutic agents currently on the market. ICG alone cannot be used for successful NIR image-guided photothermal treatment since it is volatile in aqueous solutions and therefore fails to accumulate significantly at the cancer [12,13]. The inclusion of ICG into different nanomaterials is a common strategy for improving the accumulation of ICG at the target tissue for specific tumor phototherapy, however the usage of nanomaterials coupled with the ICG are still hampered by numerous obstacles, like complex synthetic methods as well as unsolved biosafety problems [14-18]. As a result, enhancing ICG's use in photothermal cancer treatment will necessitate a new technique for improving tumor targetability.

Near-infrared fluorescence imaging together with tailored NIR fluorophores is a potential method for in vivo cancer imaging since it reduces tissue autofluorescence as well as increases the tumor-to-background ratio (TBR) [19-21]. The development of tumor-targeted NIR imaging agents is critical since the efficacy of tumor imaging relies heavily on the ability to target of NIR fluorophores with

high TBR values [22-27]. Traditional methods involve further conjugation of NIR fluorophores with tumor-targeting ligands, although chemical conjugation may affect the targetability of tumor-targeting ligands [28-30]. In order to circumvent this constraint, a novel strategy utilizing a sole NIR heptamethine cyanine dye like IR783, MHI148 (also known as IR808), or CA800SO3 has been repeatedly mentioned for structure-intrinsic tumor targeting without any need for further polymerization of tumor-targeting ligands has been developed and shown [31-33]. Because of its excellent water solubility, minimal cytotoxicity, as well as tumor-targeting specificity, IR783 is one of the most commonly utilized tumor-targeted NIR fluorophores [34-37]. There have been reports of indiscriminate absorption in healthy tissue/organs and sluggish detachment from the body up to 80 hours after injection, which pose serious obstacles to achieving adequate TBR for effective tumor imaging with the IR783 [32,33]. However, the molecular engineering for enhanced biodistribution as well as clearance that maintains tumor targetability while simultaneously enhancing TBR through quick clearance in the vivo is still critical.

An alternate strategy is by shielding ICG from its aqueous system by inclusion complexation using non-toxic cyclodextrin (CD) molecules, as biocompatibility is a crucial concern for its prospective clinical application. To increase the water stability, solubility, as well as bioavailability of hydrophobic compounds, CDs are commonly employed in pharmaceutics [38,39]. CDs are cyclic oligosaccharides that possess a hydrophobic inside and hydrophilic outside. The agglomeration as well as complexation equilibria of the connection between ICG along with methyl-cyclodextrin (Mβ-CD) in aqueous solution were discovered [40]. Many studies have employed the CD derivative Mβ-CD to eliminate cholesterol from plasma membranes because it's much more

water-soluble than Mβ-CD and has a better affinity for cholesterol removal [41,42]. Mβ-CD has also been shown to be effective in xenograft models of human cancer, according to Grosse et al [43]. A single laser irradiation with Mβ-CD and ICG combining to generate an inclusion complexation for NIR fluorescence-guided PTT has yet to be described. In order to improve the accuracy of tumor identification along with image-guided PTT, a reasonable technique to combine ICG and Mβ-CD is essential in designing a targeted phototherapeutic agent.

Although prior exertions to increase the TBR by background decrease concentrated mostly on the regulation of on/off switchable fluorescent probes through malignant environment settings, such techniques are not believed to address the underlying constraint of fluorophores, notably, their inappropriate uptake, binding, as well as retention in the tumor microenvironment [21,44-46]. According to recent findings, it is only after the development of an inclusion complex with Mβ-CD that an ICG dye may be aggressively adjusted to increase its cancer targetability along with lower its hepatic absorption [47]. The supramolecular method displayed superior in vivo performance in cancer-targeted imaging, according to preliminary research findings.

2. Materials and Methods

2. Materials and Methods

2.1. Preparation of IR783-CD Complex

All chemicals and solvents were of American Chemical Society grade or high-performance liquid chromatography (HPLC) purity. IR783 and Mβ-CD were purchased from Sigma-Aldrich (St. Louis, MO) and used as received without further purification. The IR783-CD complex was prepared using a host-guest self-assembly process. Briefly, 1 mg (1.3 μmol) of IR783 and 5 mg (3.9 μmol) of Mβ-CD were completely dissolved in 0.5 mL methanol and 1.5 mL deionized (DI) water, respectively. Next, the IR783 solution was added into the Mβ-CD aqueous solution in a dropwise manner to obtain the IR783-CD complex, followed by stirring for 6 h. The mixture was further dialyzed against DI water using a 2-kDa molecular weight cut-off membrane for 3 d to remove free IR783, Mβ-CD monomers, and residual methanol. Subsequently, the dialyzed solution was lyophilized and dispersed in phosphate-buffered saline (PBS, pH 7.4), especially for performing in vivo experiments.

2.2. Preparation of ICG-CD Complex

ICG and Mβ-CD were purchased from Sigma-Aldrich (St. Louis, MO, USA) and used as received without further purification. The ICG-CD complex was prepared using a host-guest self-assembly process. Briefly, 1 mg (1.3 μmol) of ICG and 5 mg (3.8 μmol) of Mβ-CD were completely dissolved in 0.5 mL methanol and 1.5 mL deionized (DI) water, respectively. Next, the ICG solution was added into the Mβ-CD aqueous

solution dropwise to obtain the ICG-CD complex, followed by over 6 h of stirring. The mixture was further dialyzed against DI water using a 2 kDa molecular weight cut-off membrane for 3 days to remove free ICG, Mβ-CD monomers, and residual methanol. Subsequently, the dialyzed solution was lyophilized and dispersed in phosphate-buffered saline (PBS, pH 7.4), especially important when performing in vivo experiments.

2.3. Analysis of Optical Properties

All optical measurements were performed at 37°C in PBS at pH 7.4. Absorbance and fluorescence emission spectra of free IR783 and the IR783-CD complex were measured using a fiber optic FLAME absorbance and fluorescence (200–1025 nm) spectrometer (Ocean Optics, Dunedin, FL). The fluorescence emission spectra of free ICG and the ICG-CD complex were analyzed using a SPARK® 10M microplate reader (Tecan, Männedorf, Switzerland) at an excitation wavelength of 730 nm and emission wavelengths ranging from 780 to 900 nm. Molar extinction coefficient was calculated by using the Beer–Lambert equation. To determine the fluorescence quantum yield, ICG dissolved in DMSO (quantum yield = 13%) was used as the calibration standard under the conditions of matched absorbance at 770 nm. The NIR excitation light source was provided by 5 mW of 655 nm red laser pointer (Opcom Inc., Xiamen, China) coupled with a 400 μm core diameter, NA 0.22 fiber (Ocean Optics).

2.4. In Vitro Cancer Cell Binding and NIR Fluorescence Microscopy

The human large-cell lung carcinoma cell line NCI-H460 was obtained from the American Type Culture Collection (ATCC HTB-177, Manassas, VA). The cancer cells were maintained in Roswell Park Memorial Institute

(RPMI) 1640 medium (Gibco BRL, Paisley, UK) supplemented with 10% fetal bovine serum (FBS; Gibco BRL) and an antibiotic-antimycotic solution (100 units mL^{-1} penicillin, 100 µg mL^{-1} streptomycin, and 0.25 µg mL^{-1} amphotericin B; Welgene, Daegu, South Korea) in a humidified 5% CO_2 atmosphere at 37°C. When the cells reached ≈50–60% confluence, they were then rinsed twice with PBS, the IR783-CD complex was added to each well at a concentration of 2×10^{-6} m, and cells were incubated for 24 h at 37°C. They were then gently washed with PBS. NIR fluorescence imaging was performed using a four-filter set on a Nikon Eclipse Ti-U inverted microscope system. The microscope was equipped with a 100 W halogen lamp, NIR-compatible optics, and an NIR-compatible 10× Plan Fluor objective lens (Nikon, Seoul, South Korea). Image acquisition and analysis were performed using NISElements Basic Research software (Nikon). NIR filter sets containing 750 ± 25 nm excitation filters, 785 nm dichroic mirrors, and 810 ± 20 nm emission filters were used to detect NIR fluorescence signals in cancer cells. All NIR fluorescence images were acquired at identical exposure times and normalized.

2.5. Cell Viability Assay

The cell toxicity and proliferation were evaluated by alamarBlue (Thermo Scientific, Waltham, MA) assay. The NCI-H460 cells were seeded onto 96-well plates (1 × 104 cells per well). To test cytotoxicity depending on the concentration, cancer cells were treated with the IR783-CD complex (2, 10, 25, and 50×10^{-6} m) for 1 h and cultured at 24 h post-treatment. At each assay time point, the incubation cell media was replaced with 100 µL of fresh media. 10 µL of alamarBlue solution was directly added to 100 µL each well and incubated for 4 h at 37°C in

a humidified 5% CO_2 incubator. Finally, the 96-well plates were placed into a microplate reader (SPARK 10M, Tecan, Switzerland) for measuring the absorption intensity at 570 nm and fluorescence intensity at 590 nm. The cell viability was calculated using the following formula (A is the average absorbance): cell viability (%) = (Asample − Ablank)/ (Acontrol − Ablank) × 100.

2.6. HT-29 Xenograft Mouse Model

Animal care, experiments, and euthanasia were performed in accordance with protocols approved by the Chonnam National University Animal Research Committee (CNU IACUC-H-2017-64). Adult (6-week-old) male NCRNU nude mice weighing approximately 25 g (N = 3 independent experiments) were purchased from Orient Bio Inc. (Seongnam, South Korea). HT-29 human colorectal adenocarcinoma cell line was obtained from the American Type Culture Collection (ATCC® HTB-38™). Cancer cells (1×10^{-6} cells per mouse) were harvested and suspended in 100 μL of PBS followed by subcutaneous injection into the right flank of each mouse. When the tumor size reached ~1 cm in diameter, PBS, free IR783, IR783-CD complex, free ICG, and the ICG-CD complex were administered intravenously. Animals were sacrificed and imaged over a certain period of time.

2.7. In Vivo Tumor Imaging

In vivo NIR fluorescence imaging was performed using a fluorescence imaging system (FOBI, NeoScience, Suwon, South Korea). At 4 and 24 h post-injection, the mice were sacrificed and their main organs (heart, lungs, liver, pancreas, spleen, kidneys, duodenum, and intestine) were collected and imaged to evaluate the time-dependent biodistribution of

free IR783 and the IR783-CD complex. Fluorescence intensities accumulated in tumor and organs were analyzed using ImageJ version 1.45q (National Institutes of Health, Bethesda, MD). The TBR was calculated as fluorescence/ background, where background was the signal intensity of a region adjacent to the tumor over the imaging period. All NIR fluorescence images were normalized identically for all conditions.

To confirm the in vivo antitumor effect, the macroscopic features of each group were observed at fixed time intervals for a week. The tumor volumes were calculated using the following formula: $V = 0.5 \times$ longest diameter $\times$ (shortest diameter)^2.

2.8. Assessment of In Vivo Photothermal Effect

HT-29 tumor-bearing mice were intravenously administered with PBS, free ICG, and the ICG-CD complex. At 4 h after injection, the mice were anesthetized, and their tumor sites were laser-irradiated (1.1 W/cm^2, λ = 808 nm) for 5 min. Temperature changes in the tumor sites were monitored using a FLIR® thermal imager (FLIR Systems, Wilsonville, OR, USA) and data were recorded from the beginning of the laser irradiation at a step-size of 1 min during the entire laser irradiation period. At 24 h post-irradiation, tumors were excised from the treated mice for subsequent histological analysis using hematoxylin and eosin (H&E) staining.

2.9. Statistical Analysis

Statistical analysis was carried out using a one-way ANOVA followed by Tukey's multiple comparisons test. Differences were considered statistically significant at a level of $p < 0.05$. Results are presented as the mean ± S.D. and curve fitting was performed using Prism version

4.0a software (GraphPad, San Diego, CA, USA).

2.10. Histological Analysis and NIR Fluorescence Microscopy

Resected tumors were preserved for performing hematoxylin and eosin (H&E) staining and NIR fluorescence microscopic assessment. Briefly, samples were fixed in 2% paraformaldehyde (PFA) and flash frozen in optimal cutting temperature (OCT) compound using liquid nitrogen. Frozen samples were cryosectioned (at a thickness of 10 μm per slide), observed by fluorescence microscopy, and then stained with H&E. NIR imaging was performed using a four-filter set of the Nikon Eclipse Ti-U inverted microscope system (Nikon). Image acquisition and analysis were performed using the NIS-Elements Basic Research software (Nikon). All NIR fluorescence images had identical exposure time and normalization.

3. Results and Discussion

3.1. Preparation and Characterization of the IR783-CD Complex

Although IR783 by itself and IR783-drug conjugates have been widely used for tumor-targeted imaging and therapy due to the structure-inherent tumor targeting capability of IR783, the in vivo performance was suboptimal due to their high non-specific background uptake. Due to the presence of anionic sulfonyl side chains on the indolenine nucleus, IR792 is a well-defined hydrophilic tricarbocyanine dye. As such, it results in a relatively higher non-specific uptake in normal tissues/organs and slower biodistribution and clearance. An IR783-CD complex was designed to improve the in vivo performance of IR783 for rapid biodistribution and clearance of IR783 against tumors. This led to improved tumor-targeted imaging with a high TBR. Figure 1a describes the schematic preparation of the IR783-CD complex. As previously demonstrated, the Mβ-CD has significant advantages after forming inclusion complexes with the heptamethine cyanine dye such as water stability and bioavailability. As such, we expected that the IR783-CD complex would exhibit rapid biodistribution and clearance after intravenous administration and as a result, would achieve a higher TBR for improved tumor imaging. Figure 1b summarizes that the optical properties of the IR783-CD complex measured in phosphate-buffered saline (PBS, pH 7.4) were similar to those of free IR783 with the exception of the higher quantum yield (Φ = 5.4%). The absorbance of the IR783-CD complex at 700 nm (also known as dimer λmax) reduced whereas the fluorescence intensity of the IR783-CD complex increased than that of free IR783 under the same condition (Figure 2). This suggests that the Mβ-CD may assist in preventing dimeric aggregation of

IR783 after forming inclusion complexes with free IR783. More importantly, the rapid body clearance within twenty four hours post-injection was apparently induced by the IR783-CD complex compared to the 80 h of free IR783. The results show that under aqueous conditions, the IR783-CD complex was successfully prepared by a host–guest self-assembly process and that the Mβ-CD may be able to improve the water stability and optical properties of IR783 as well as total body clearance.

3.2 In Vitro Cellular Uptake and Cytotoxicity

NCI-H460 cancer cells were used for the in vitro study to assess the cytocompatibility of the IR783-CD complex and the cellular uptake. To evaluate cytotoxicity, alamarBlue assay was performed to determine the relative viability of NCI-H460 cancer cells after incubation with the IR783-CD complex at various concentrations (2, 10, 25, and 50×10^{-6} m) for twenty four hours. Even with the high concentration of 50×10^{-6} m IR783-CD complex, no significant cytotoxicity was observed as seen in Figure 3a. This shows that the IR783-CD complex does not induce obvious toxicity. Furthermore, by measuring fluorescence signals in NCI-H460 cells after incubation with the IR783-CD complex for twenty four hours, intracellular distribution of the IR783-CD complex was confirmed (Figure 3b). At twenty four hours post-treatment, significant NIR fluorescence was observed in the cancer cells which demonstrate the intracellular localization of the IR783-CD complex.

3.3. Time-Dependent In Vivo Biodistribution and Clearance

Next, we investigated the time-dependent biodistribution and clearance of free IR783 and the IR783-CD complex in mice. For ten minutes, the

initial distribution was continuously monitored by the real-time NIR fluorescence imaging system immediately after a single intravenous injection of free IR783 or the IR783-CD complex (10 nmol, 0.3 mg kg^{-1} calculated using the IR783 concentration). Overall, both injections resulted in equal distribution in the blood, heart, lungs, liver, and other major organs within one hour post-injection and then continued to accumulate into the liver, followed by hepatobiliary and intestinal excretion. The NIR fluorescence signals of the IR783-CD complex were primarily located in the gastrointestinal tract at four hours post-injection (Figure 4a). Surprisingly, the IR783-CD complex showed incredibly high fluorescence in the intestines and feces due to rapid excretion through the biliary and intestinal routes within four hours post-injection. In contrast, at four hour post-injection, free IR783 exhibited high non-specific uptake in almost every tissue and organ in the body. These results indicate that the IR783-CD complex could quickly excrete into the small intestine, especially in the feces, within four hours post-injection and avoid non-specific uptake by the reticuloendothelial system (RES). Even though the reason for this observation is not fully understood, Mβ-CD moieties of the ICG-CD complex most likely minimizes the interaction with plasma proteins through molecular shielding unlike that observed with free IR783. The IR783-CD complex appeared to be eliminated through the intestinal routes with no appreciable non-specific background signal in any of the tissues or organs with only a negligible signal remaining in the liver. Free IR783 on the other hand, remained throughout the body without additional excretion. Furthermore, the fluorescence intensities that remained in the resected tissues and organs were measured at four and twenty four hours post-injections of free IR783 and the IR783-CD complex and were compared to measure the difference of time-dependent biodistribution and clearance (Figure 4b). As the experiments focused on lowering the

non-specific background fluorescence, this method was readily applicable in combination with various types of carbocyanine-based dyes for improved NIR fluorescence imaging.

3.4. Time-Dependent In Vivo Tumor Imaging

The tumor imaging capability of the IR783-CD complex in vivo was investigated in the NCIH460 xenograft tumor model after confirming the rapid biodistribution and clearance of the IR783-CD complex. Real-time NIR fluorescence imaging was performed for twenty four hours post-injection after a single dose of either the free IR783 or IR783-CD complex (10 nmol, 0.3 mg kg^{-1} calculated using the IR783 concentration) was intravenously administered into tumor-bearing mice (Figure 5a). The time-dependent NIR fluorescence imaging showed that the fluorescence intensity at the tumor site upon treatment with free IR783 reached a maximum at four hours post-injection whereas the fluorescence signal from the tumor injected with the IR783-CD complex maintained a constant level without peak accumulation until after twenty four hours of administration (Figure 5b). The background fluorescence caused by nonspecific uptake of free IR783 in adjacent regions to the tumor however, was higher than the background signals of the IR783-CD complex which indicated that the free IR783 had lower specificity and selectivity. More importantly, the TBR values of the IR783-CD complex gradually increased over twenty four hours post-injection and remained higher than that of free IR783 (Figure 5c). As it is challenging to obtain an adequate TBR value for most tumor-targeting contrast agents, this finding was important for intraoperative optical imaging for improved image-guided surgery and in performing diagnostic imaging for early and accurate cancer detection. Furthermore, tumors were resected

subsequently along with other tissues and organs, their fluorescence signals were compared against that of a muscle, and went through histological analysis and NIR fluorescence microscopy (Figure 6). As expected, the fluorescence signal of the IR783-CD complex in the tumor tissue was similar to that of free IR783 because of the similarities of their tumor affinities, extinction coefficients, and quantum yields. The combined use of IR783 and Mβ-CD allows rapid biodistribution and clearance within twenty four hours post-injection, has lower non-specific uptake by the RES, and has higher TBR which allows improved target detectability and imaging.

3.5. Preparation and Characterization of the ICG-CD Complex

ICG can form dimers and oligomers in aqueous solutions because it has presence of hydrophilic sulfonyl and hydrophobic naphthyl groups in its chemical structure and is a conventional amphiphilic tricarbocyanine dye. When ICG aggregates, it causes self-quenching. This results in a reduction of fluorescence intensity in aqueous solutions. An ICG-CD complex was designed to overcome the low water stability and tumor targetability. This complex helps improve the in vivo bioavailability of ICG against tumors for application in targeted photothermal cancer treatment. The ICG-CD complex preparation is described more in Figure 7. Inclusion complexes comprising of Mβ-CD has many advantages such as stability, improved water solubility, and bioavailability. As such, we have expected that the ICG-CD complex could achieve high tumor accumulation for enhanced PTT due to a high optical and chemical stability. Figure 8a shows that when under the same conditions, the absorption peaks of the ICG-CD complex that were measured in PBS were similar to those of ICG between the wavelengths of 710 nm and 780 nm. More importantly,

the intensity of the absorption peak of the ICG-CD complex at 780 nm (known as monomer λmax) significantly increased while the absorbance of the ICG-CD complex at 710 nm (known as dimer λmax) reduced when compared to with the same concentration of free ICG. These results indicate that Mβ-CD could play an important role in preventing the dimeric aggregation of ICG after inclusion complexes with free ICG are formed. Furthermore, under the same conditions, the ICG-CD complex showed significant higher fluorescence intensity than free ICG as shown in Figure 8b. As a result, this demonstrates that in aqueous solution, the ICG-CD complex was successful in using a host-guest self-assembly process and that the Mβ-CD may help in improving the stability and optical properties of ICG in water.

3.6. Assessment of In Vitro Photothermal Effect

An important prerequisite for successful therapeutic efficacy of a photothermal agent is to have an efficient light-to-heat conversion. Temperature changes were continuously recorded using a FLIR® thermal imager as the ICG-CD complex solution (100 μM, which is equivalent to a 0.3 mg/kg single dose of free ICG), PBS, and free ICG were irradiated by an 808 nm NIR laser (1.1 W/cm^2) for one minute. The temperature change of the ICG-CD complex was similar to that of the free ICG solution, as expected. The temperature of the ICG-CD complex solution immediately increased from room temperature (25.6°C) to 89.1°C and after one minute of irradiation, only a minor change was observed for PBS (Figure 9a). The ICG-CD complex showed a rapid increase in temperature (~80°C) within the first 30 seconds and the temperature plateaued within one minute of laser irradiation (Figure 9b). These results indicate that the ICG-CD complex could potentially be an effective PTT

agent for photothermal cancer treatment. In addition, the absorbance of the ICG-CD complex at 780 nm gradually reduced upon prolonged irradiation with the 808 nm laser (1.1 W/cm^2) for five minutes. This indicates that after the completion of light-to-heat conversion performance, ICG was photobleached (Figure 9c).

3.7. In Vivo NIR Fluorescence Imaging for Tumor Targetability

To identify the biodistribution behavior and in vivo tumor targetability of free ICG and the ICG-CD complex in HT-29 xenograft tumor models, real-time NIR fluorescence imaging was performed. Tumor-bearing mice were intravenously injected with either a single dose of free ICG or the ICG-CD complex (10 nmol, 0.3 mg/kg calculated using the ICG concentratrion) and were imaged at different points in time to investigate the accumulation of the ICG-CD complex at the tumor sites with that of the free ICG as reflected in Figure 10a. Results from the time-dependent NIR fluorescence imaging showed that the fluorescence intensity at the tumor site upon treatment with the ICG-CD complex reached its maximum at four hours post-injection whereas the tumor injected with free ICG showed a continuous decrease without peak accumulation until after twenty four hours after administration (Figure 10b). The results of this study show that the Mβ-CD moieties of the ICG-CD complex play an important role in improving tumor targeting; as such, the ICG-CD complex may be used for enhanced photothermal cancer treatment. In addition, we monitored the fluorescence signals in the major organs that were collected from mice after four hours from injection to confirm the biodistribution of free ICG and the ICG-CD complex (Figure 10c, d). As expected, we detected free ICG uptake in the duodenum, liver, and intestinal tract due to hepatobiliary clearance, which is a well-known

characteristic of ICG. In contrast, with the exception of the liver, ICG-CD complex uptake was similar to that of free ICG in the intestinal tract and duodenum. More importantly, a consequence of the reticuloendothelial system-stealthy feature of Mβ-CD could be a differential uptake in the liver between the ICG-CD complex and free ICG. Because Mβ-CD may help in improving the stability and water solubility of ICG, the ICG-CD complex could leave the liver and achieve prolonged blood circulation which may result in preferential tumor uptake.

3.8. Assessment of In Vivo Photothermal Effect

The PTT capability of the complex in vivo was investigated in the HT-29 xenograft tumor model after the photothermal effect of the ICG-CD complex in vitro was confirmed. Four hours prior to 808 nm laser irradiation (1.1 W/cm² for 5 min), a single dose of the ICG-CD complex (10 nmol based on the ICG concentration) was intravenously injected into tumor-bearing mice. Additionally, to verify the photothermal effect generated by only laser power, free ICG and PBS were tested separately under the same conditions. Variations in temperature were recorded each minute at the tumor sites in each group using a FLIR® thermal imager. Under laser irradiation, a rapid increase in tumor temperature (~56.2°C) was detected in the ICG-CD complex-treated group, whereas a small increase in temperature was noticed in the PBS- or free ICG-injected groups (~40.3°C and ~45.1°C respectively) (Figure 11a). The results of this study suggest that the marked change in temperature on the tumor tissue was mediated by the improved tumor targetability of the ICG-CD complex. Within two minutes of laser irradiation, the tumor temperature in ICG-CD complex-treated mice increased rapidly to ~51°C which was sufficient to induce complete tumor

necrosis. In contrast, the tumor temperatures in other groups were within the range of 40–45°C until five minutes, which was insufficient for tumor suppression (Figure 11b).

3.9. In Vivo PTT Efficacy

The ICG-CD complex was determined to be suitable for use as a highly efficient phototherapeutic agent for fluorescence-guided PTT in tumor-bearing mice due to its excellent vitro photothermal effect and improved tumor accumulation in vivo. To determine the antitumor effect of the ICG-CD complex, tumor growth in HT-29 xenograft tumor models was monitored continuously for nine days after PTT (Figure 12a). To reflect the change in tumor size, representative images of mice from each group were acquired. During an observation period of nine days, tumor volumes in the ICG-CD complex-treated group decreased rapidly without tumor regrown within five days of laser irradiation, whereas tumor volumes of the groups treated with PBS and free ICG prior to laser irradiation increased three to four-folds (Figure 12b). The combination of the ICG-CD complex and laser irradiation induced tumor ablation resulted in only black scars at the tumor site after three days of treatment due to improved accumulation of the ICG-CD complex at the tumor sites. Furthermore, no body weight loss was observed in the tumor mice during the course of the therapy which indicates that the treatment was safe and harmless (Figure 12c). Additional evaluation was conducted by H&E staining of tumor tissue samples that were collected from each group after one day of treatment (Figure 12d). Groups treated with the combination of laser irradiation and the ICG-CD complex showed significant cell damage including nuclear damage and cell shrinkage. In contrast, vigorous cell proliferation and tight arrangements without any

detectable damage was present in tumor tissues from other groups. As a result, this demonstrates that the ICG-CD complex is promising for effective cancer phototherapy.

4. Conclusion

Briefly stated, a quick physique-clearable IR783-CD complex was effectively generated using the host-guest addition complexation of IR783 and Mβ-CD in an aqueous solution, and so this complex was then employed in studies to enhance malignancy imaging for fluorescence-guided operations. A greater TBR value was found at the tumor location with the combination of IR783 and CD than with free IR783. Within 24 hours of intravenous administration, Mβ-CD enhanced the removal of IR783 from the body, increasing its tumor imaging capability. This methodology presents a practical, easy, effective, as well as field-applicable solution for overcoming the constraints associated with the presently available tricarbocyanine dyes, while remaining basic and straightforward. When coupled with other carbocyanine dyes for malignancy imaging, Mβ-CDs serve a vital role in minimizing nonspecific background signal. Through host-guest incorporation complexation of the ICG as well as the Mβ-CD in an aqueous condition, it was finally possible to construct a phototherapeutic ICG-CD complex, which was then employed to boost tumor accumulation for improved photothermal performance. Compared to free ICG, the ICG-CD complex performed better in targeted tumor imaging. ICG's PTT effectiveness was further enhanced since Mβ-CD made it easier for the drug to target tumors. Cancer PTT guided by fluorescence was shown to be very successful, resulting in apparent tumor elimination without injuring neighboring normal tissues, according to the results. As a result, the ICG-CD complex has the potential to be a viable phototherapeutic agent in the future for specific cancer imaging as well as precision cancer PTT in clinical settings.

References

1. Zhu, H.; Cheng, P.; Chen, P.; Pu, K. Recent progress in the development of near-infrared organic photothermal and photodynamic nanotherapeutics. Biomater. Sci. 2018, 6, 746-765.
2. Li, J.; Pu, K. Development of organic semiconducting materials for deep-tissue optical imaging, phototherapy and photoactivation. Chem. Soc. Rev. 2019, 48, 38-71.
3. Cho, M.H.; Li, Y.; Lo, P.; Lee, H.; Choi, Y. Fucoidan-based theranostic nanogel for enhancing imaging and photodynamic therapy of cancer. Nano-Micro Lett. 2020, 12, 47.
4. Yoo, Y.; Jo, G.; Jung, J.S.; Yang, D.H.; Hyun, H. Multivalent sorbitol probes for near-infrared photothermal cancer therapy. Part. Part. Syst. Charact. 2020, 37, 1900490.
5. Lim, W.; Jo, G.; Kim, E.J.; Cho, H.; Park, M.H.; Hyun, H. Zwitterionic near-infrared fluorophore for targeted photothermal cancer therapy. J. Mater. Chem. B 2020, 8, 2589-2597.
6. Park, M.H.; Jo, G.; Kim, E.J.; Jung, J.S.; Hyun, H. Tumor-targeted near-infrared fluorophore for fluorescence-guided phototherapy. Chem. Commun. 2020, 56, 4180-4183.
7. Lee, S.; Jo, G.; Jung, J.S.; Yang, D.H.; Hyun, H. Near-infra-red fluorescent chitosan oligosaccharide lactate for targeted cancer imaging and photothermal therapy. Artif. Cells Nanomed. Biotechnol. 2020, 48, 1144-1152.
8. Lee, S.; Jung, J.S.; Jo, G.; Yang, D.H.; Koh, Y.S.; Hyun, H. Near-infrared fluorescent sorbitol probe for targeted photothermal cancer therapy. Cancers 2019, 11, 1286.
9. Feng, B.; Niu, Z.; Hou, B.; Zhou, L.; Li, Y.; Yu, H. Enhancing triple negative breast cancer immunotherapy by ICG-templated self-assembly of paclitaxel nanoparticles. Adv. Funct. Mater. 2020, 30, 1906605.
10. Quan, Y.H.; Oh, C.H.; Jung, D.; Lim, J.Y.; Choi, B.H.; Rho, J.; Choi, Y.;

Han, K.N.; Kim, B.M.; Kim, C.; et al. Evaluation of intraoperative near-infrared fluorescence visualization of the lung tumor margin with indocyanine green inhalation. JAMA Surg. 2020, 155, 732-740.

11. Yu, S.; Cheng, B.B.; Yao, T.F.; Xu, C.C.; Nguyen, K.T.; Hong, Y.; Yuan, B.H. New generation ICG-based contrast agents for ultrasound-switchable fluorescence imaging. Sci. Rep. 2016, 6, 35942.
12. Shan, W.J.; Chen, R.H.; Zhang, Q.; Zhao, J.; Chen, B.B.; Zhou, X.; Ye, S.F.; Bi, S.L.; Nie, L.M.; Ren, L. Improved stable indocyanine green (ICG)-mediated cancer optotheranostics with naturalized hepatitis B core particles. Adv. Mater. 2018, 30, 1707567.
13. Kirchherr, A.K.; Briel, A.; Mäder, K. Stabilization of indocyanine green by encapsulation within micellar systems. Mol. Pharm. 2009, 6, 480-491.
14. Liu, R.; Yao, T.; Liu, Y.; Yu, S.; Ren, L.; Hong, Y.; Nguyen, K.T.; Yuan, B. Temperature-sensitive polymeric nanogels encapsulating with β -cyclodextrin and ICG complex for high-resolution deep-tissue ultrasound-switchable fluorescence imaging. Nano Res. 2020, 13, 1100-1110.
15. An, F.; Yang, Z.; Zheng, M.; Mei, T.; Deng, G.; Guo, P.; Li, Y.; Sheng, R. Rationally assembled albumin/indocyanine green nanocomplex for enhanced tumor imaging to guide photothermal therapy. J. Nanobiotechnol. 2020, 18, 49.
16. Lin, H.; Li, S.; Wang, J.; Chu, C.; Zhang, Y.; Pang, X.; Lv, P.; Wang, X.; Zhao, Q.; Chen, J.; et al. A single-step multi-level supramolecular system for cancer sonotheranostics. Nanoscale Horiz. 2019, 4, 190-195.
17. Guerrini, L.; Hartsuiker, L.; Manohar, S.; Otto, C. Monomer adsorption of indocyanine green to gold nanoparticles. Nanoscale 2011, 3, 4247-4253.
18. Zhou, J.; Meng, L.; Sun, C.; Ye, W.; Chen, C.; Du, B. A “protective umbrella” nanoplatform for loading ICG and multi-modal imaging-guided phototherapy. Nanomedicine 2018, 14, 289-301.
19. H. Kobayashi, M. Ogawa, R. Alford, P. L. Choyke, Y. Urano, Chem. Rev. 2010, 110, 2620..

20. Y. Ye, X. Chen, Theranostics 2011, 1, 102.
21. H. S. Choi, S. L. Gibbs, J. H. Lee, S. H. Kim, Y. Ashitate, F. Liu, H. Hyun, G. Park, Y. Xie, S. Bae, M. Henary, J. V. Frangioni, Nat. Biotechnol. 2013, 31, 148.
22. H. Hyun, M. H. Park, E. A. Owens, H. Wada, M. Henary, H. J. M. Handgraaf, A. L. Vahrmeijer, J. V. Frangioni, H. S. Choi, Nat. Med. 2015, 21, 192.
23. H. Hyun, H. Wada, K. Bao, J. Gravier, Y. Yadav, M. Laramie, M. Henary, J. V. Frangioni, H. S. Choi, Angew. Chem., Int. Ed. 2014, 53, 10668.
24. H. Hyun, E. A. Owens, M. H. Park, H. Wada, J. V. Frangioni, M. Henary, H. S. Choi, Angew. Chem., Int. Ed. 2015, 54, 8648.
25. E. A. Owens, M. Henary, G. E. Fakhri, H. S. Choi, Acc. Chem. Res. 2016, 49, 1731.
26. G. Y. Pan, H. R. Jia, Y. X. Zhu, R. H. Wang, F. G. Wu, Z. Chen, ACS Biomater. Sci. Eng. 2017, 3, 3596.
27. G. Gao, Y. W. Jiang, W. Sun, Y. Guo, H. R. Jia, X. W. Yu, G. Y. Pan, F. G. Wu, Small 2019, 15, 1900501.
28. C. Shi, J. B. Wu, D. Pan, J. Biomed. Opt. 2016, 21, 050901.
29. S. Luo, E. Zhang, Y. Su, T. Cheng, C. Shi, Biomaterials 2011, 32, 7127.
30. D. W. Hwang, M. J. Jo, J. H. Lee, H. Kang, K. Bao, S. Hu, Y. Baek, H. G. Moon, D. S. Lee, S. Kashiwagi, M. Henary, H. S. Choi, Adv. Ther. 2019, 2, 1900111.
31. L. Duan, L. Wang, C. Zhang, L. Yu, F. Guo, Z. Sun, Y. Xu, F. Yan, Int. J. Clin. Exp. Pathol. 2019, 12, 2353.
32. X. Yang, C. Shi, R. Tong, W. Qian, H. E. Zhau, R. Wang, G. Zhu, J. Cheng, V. W. Yang, T. Cheng, M. Henary, L. Strekowski, L. W. K. Chung, Clin. Cancer Res. 2010, 16, 2833.
33. M. H. Park, G. Jo, E. J. Kim, J. S. Jung, H. Hyun, Chem. Commun. 2020, 56, 4180.
34. Y. Guan, Y. Zhang, J. Zou, L. P. Huang, M. D. Chordia, W. Yue, J. J.

Wu, D. F. Pan, Molecules 2019, 24, 4120.

35. V. S. R. Harrison, C. E. Carney, K. W. MacRenaris, E. A. Waters, T. J. Meade, J. Am. Chem. Soc. 2015, 137, 9108..

36. A. Yuan, J. Wu, X. Tang, L. Zhao, F. Xu, Y. Hu, J. Pharm. Sci. 2013, 102, 6..

37. S. Siriwibool, N. Kaekratoke, K. Chansaenpak, K. Siwawannapong, P. Panajapo, K. Sagarik, P. Noisa, R. Y. Lai, A. Kamkaew, Sci. Rep. 2020, 10, 1283..

38. Kurahashi, T.; Iwatsuki, K.; Onishi, T.; Arai, T.; Teranishi, K.; Hirata, H. Near-infrared indocyanine dye permits real-time characterization of both venous and lymphatic circulation. J. Biomed. Opt. 2016, 21, 086009.

39. Szente, L.; Szejtli, J. Highly soluble cyclodextrin derivatives: Chemistry, properties, and trends in development. Adv. Drug Deliv. Rev. 1999, 36, 17–28.

40. Barros, T.C.; Toma, S.H.; Toma, H.E.; Bastos, E.L.; Baptista, M.S. Polymethine cyanine dyes in β-cyclodextrin solution: Multiple equilibria and chemical oxidation. J. Phys. Org. Chem. 2010, 23, 893–903.

41. Onodera, R.; Motoyama, K.; Okamatsu, A.; Higashi, T.; Arima, H. Potential use of folate-appended methyl-β-cyclodextrin as an anticancer agent. Sci. Rep. 2013, 3, 1104.

42. Loftsson, T.; Brewster, M.E. Pharmaceutical applications of cyclodextrins: Basic science and product development. J. Pharm. Pharmacol. 2010, 62, 1607–1621.

43. Grosse, P.Y.; Bressolle, F.; Pinguet, F. Antiproliferative effect of methyl-b-cyclodextrin in vitro and in human tumour xenografted athymic nude mice. Br. J. Cancer 1998, 78, 1165–1169.

44. H. S. Choi, K. Nasr, S. Alyabyev, D. Feith, J. H. Lee, S. H. Kim, Y. Ashitate, H. Hyun, G. Patonay, L. Strekowski, M. Henary, J. V. Frangioni, Angew. Chem., Int. Ed. 2011, 50, 6258.

45. A. Mochida, F. Ogata, T. Nagaya, P. L. Choyke, H. Kobayashi, Bioorg. Med. Chem. 2018, 26, 925..

46. Y. Urano, D. Asanuma, Y. Hama, Y. Koyama, T. Barrett, M. Kamiya, T. Nagano, T. Watanabe, A. Hasegawa, P. L. Choyke, H. Kobayashi, Nat. Med. 2009, 15, 104..

47. G. Jo, B. Y. Lee, E. J. Kim, M. H. Park, H. Hyun, Biomedicines 2020, 8, 476.

48. H. Hyun, M. W. Bordo, K. Nasr, D. Feith, J. H. Lee, S. H. Kim, Y. Ashitate, L. A. Moffitt, M. Rosenberg, M. Henary, H. S. Choi, J. V. Frangioni, Contrast Media Mol. Imaging 2012, 7, 516..

근적외선 형광조영제와 사이클로덱스트린 복합체를 이용한 종양 이미징과 광열치료기법

이 보 영

전남대학교대학원 의과학과 의생명학전공

(지도교수 : 현 훈)

국문초록

표적 근적외선(NIR) 형광체를 사용한 NIR 형광 암 이미징은 정확한 검출 및 암 진단에 유용하다. IR783과 메틸-β-사이클로덱스트린(Mβ-CD) 복합체는 빠른 전신 생체 분포를 가능하게 하여 비특이적 배경 흡수를 현저하게 감소시켰고, 따라서 주입 후 24시간 이내에 Tumor-to-background ratio(TBR) 값을 증가시켰다. 또한, 인도시아닌 그린(ICG)과 메틸-β-사이클로덱스트린(Mβ-CD)은 free ICG보다 표적 종양 이미징에서 더 높은 효과를 나타냈으며, 종양 표적화를 촉진하여 PTT의 효능을 더욱 증가시켰다. NIR 레이저 조사 시 ICG-CD 복합체에 의해 가해진 광열 효과는 5분 이내에 종양 부위의 온도를 56.2℃까지 크게 향상시켰으며 9일 후 종양 부피가 눈에 띄게 감소했다. 따라서 IR783 및 ICG-CD 복합체는 임상에서 빠르고 정확한 진단과 인접한 조직을 손상시키지 않고도 확실한 종양 절제를 하여 안전하고 획기적인 암 치료 방법으로 활용할 수 있다.

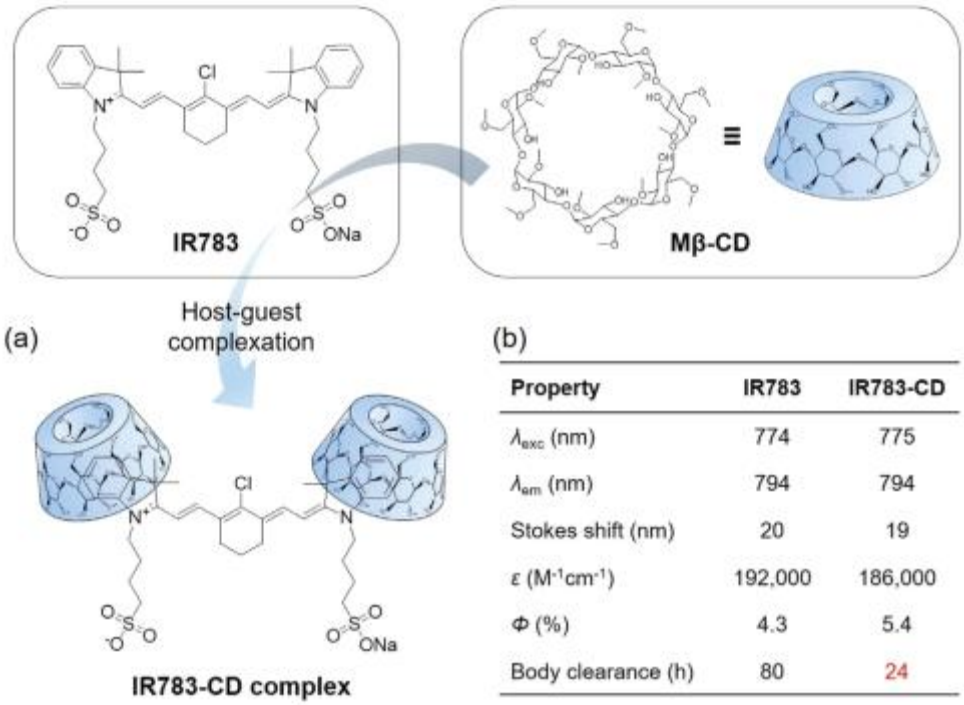

(a)

(b)

Property	IR783	IR783-CD
λ_{exc} (nm)	774	775
λ_{em} (nm)	794	794
Stokes shift (nm)	20	19
ε ($M^{-1}cm^{-1}$)	192,000	186,000
Φ (%)	4.3	5.4
Body clearance (h)	80	24

Figure 1. (a) This is a schematic representation of inclusion complex formation between IR783 and Mβ-CD in an aqueous solution. **(b)** Table that compares the optical property and in vivo performance between free IR783 and the IR783-CD complex. Optical measurements were performed in PBS at pH 7.4.

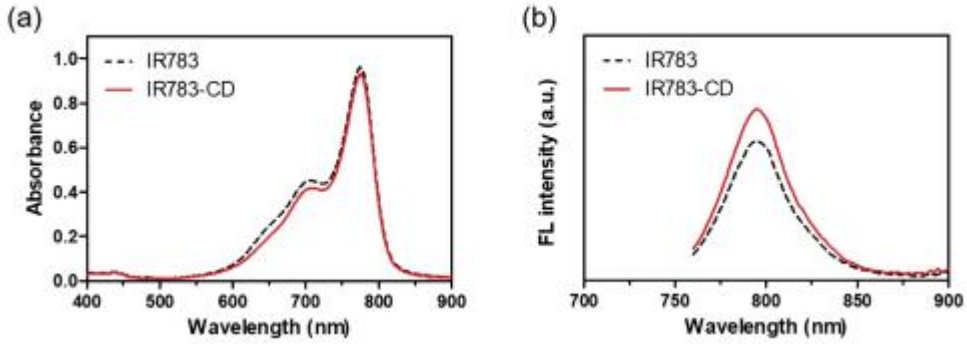

Figure 2. Graphs showing the optical properties of free IR783 and the IR783-CD complex. Changes in (a) absorbance and (b) fluorescence spectra of IR783 and IR783-CD solutions at equal IR783 concentrations. Absorbance and fluorescence emission spectra of each sample were obtained at a fixed IR783 concentration of 5×10^{-6} m in PBS at pH 7.4.

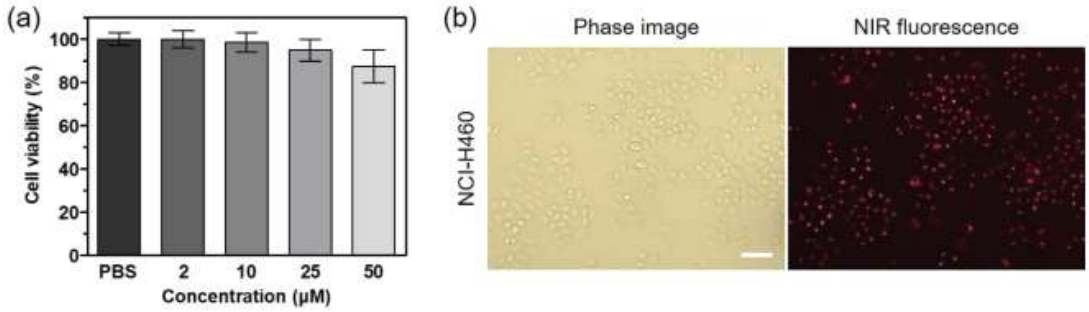

Figure 3. (a) Graph of cell viability assay of the IR783-CD complex using NCI-H460 cancer cells. Cyto-compatibility was plotted with various concentrations of the IR783-CD complex twenty four hours post-treatment. Data is expressed as the mean ± SD of the three independent experiments. (b) Live cancer cell binding of the IR783-CD complex in NCI-H460 cells. Phase contrast and NIR fluorescence images of the cell line were obtained at an IR783-CD concentration of 2×10^{-6} m. The sample concentration is calculated using the absorbance value of the IR783. Images are representative of three independent experiments. The NIR fluorescence image has identical exposure time and normalization. Each scale bar represents 100 μm.

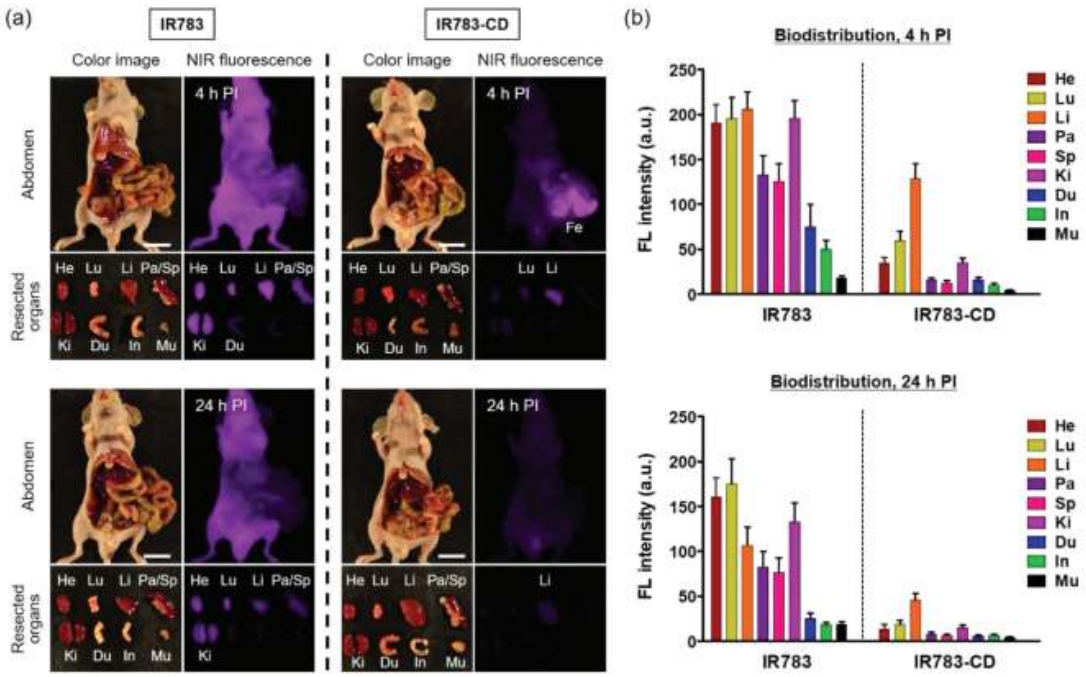

Figure 4. Time-dependent in vivo biodistribution of free IR783 and the IR783-CD complex. **(a)** Imaging of abdominal exploration and resected organs imaged at four and twenty four hours post-injections of IR783 and the IR783-CD complex. **(b)** Quantitative fluorescence analysis of intraoperative dissected organs at four and twenty four hours post-injections of IR783 and the IR783-CD complex. Mice were intravenously injected with 10 nmol of either the IR783 or IR783-CD complex and were imaged for twenty four hours. Abbreviations: Du, duodenum; Fe, feces; He, heart; In, intestine; Ki, kidneys; Li, liver; Lu, lungs; Mu, muscle; Pa, pancreas; Sp, spleen; and PI, post-injection. Each scale bar represents 1 centimeter. Images are representative of three independent experiments. All NIR fluorescence images have identical exposure time and normalizations. Data is expressed as the mean ± SD of the three independent experiments.

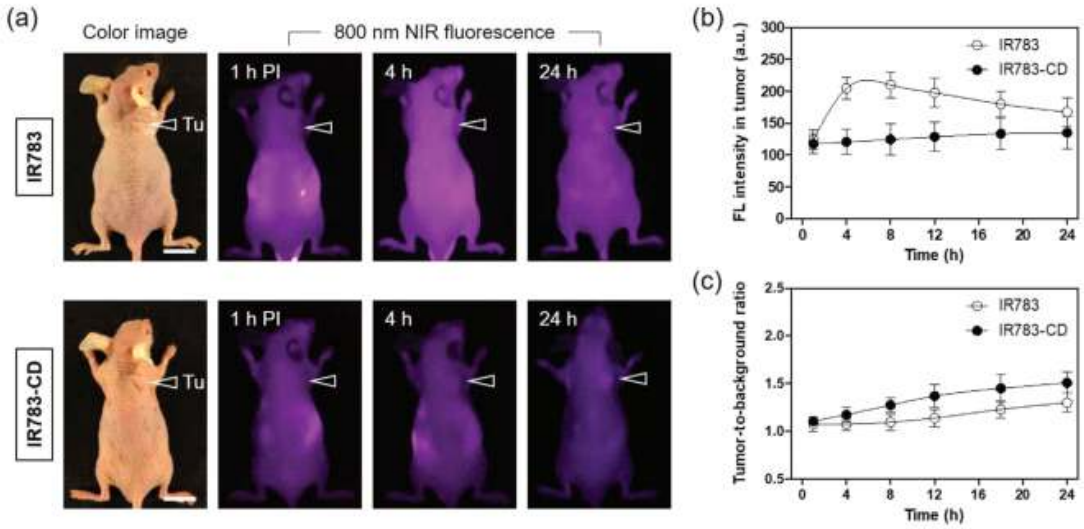

Figure 5. Time-dependent in vivo tumor imaging of free IR783 and the IR783-CD complex. (a) Reflects the NIR fluorescence imaging twenty four hours post-injection of IR783 and the IR783-CD complex. (b) Graph reflecting the time-dependent fluorescence intensity at tumor sites targeted by IR783 and the IR783-CD complex. (c) Reflects the time course of TBR for twenty four hours post-injection of IR783 and the IR783-CD complex. TBR was calculated as the fluorescence intensity of tumor tissue compared to the signal intensity of neighboring tissue obtained at different time points. Abbreviations: PI, post-injection; and Tu, tumor. Each scale bar represents 1 centimeter. Images are representative of three independent experiments. All NIR fluorescence images have identical exposure time and normalizations. Data is expressed as the mean ± SD of three independent experiments.

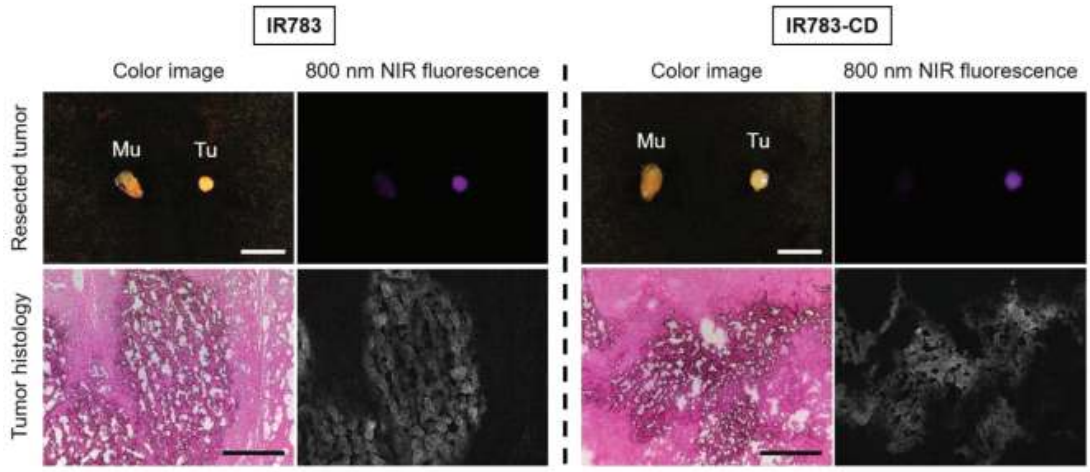

Figure 6. Tumor sections resected from the mice injected with IR783 and the IR783-CD complex at 24 h post-injection, respectively (top). Histological analysis of the resected tumor tissues stained with H&E at 24 h after injection of IR783 and the IR783-CD complex (bottom). Abbreviations: Mu, muscle; and Tu, tumor. Scale bars = 1 cm (white bars) and 300 μm (black bars). Images are representative of three independent experiments. All NIR fluorescence images have identical exposure time and normalizations.

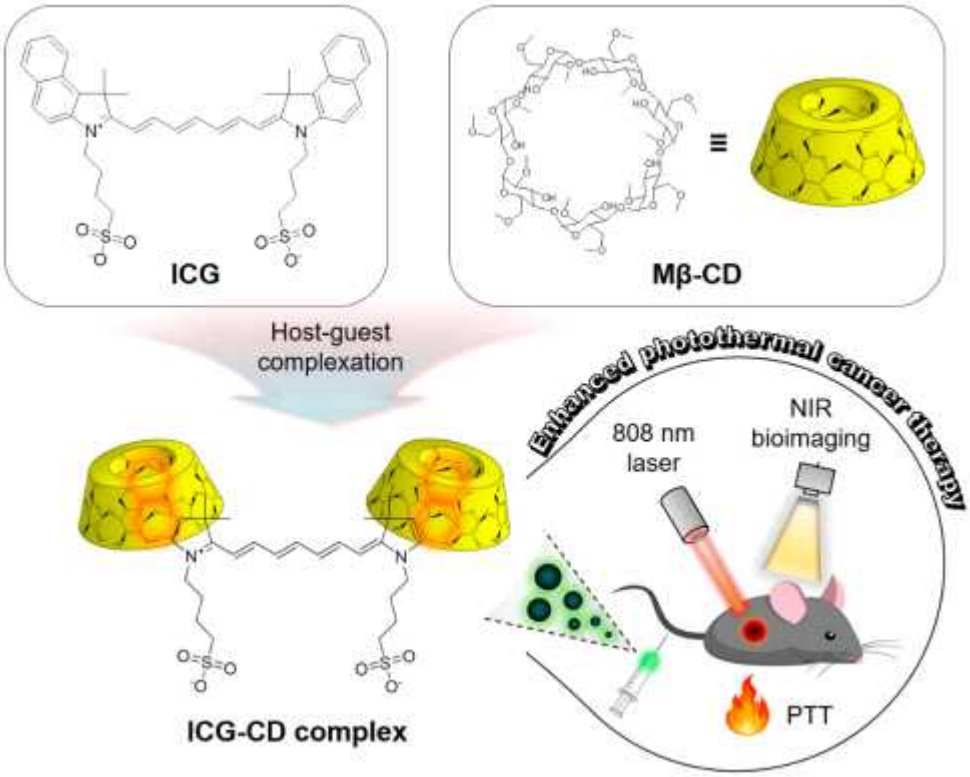

Figure 7. This figure shows a schematic representation of inclusion complex formation between indocyanine green (ICG) and methyl-β-cyclodextrin (Mβ-CD) in an aqueous state for enhanced photothermal cancer therapy. PTT: photothermal therapy.

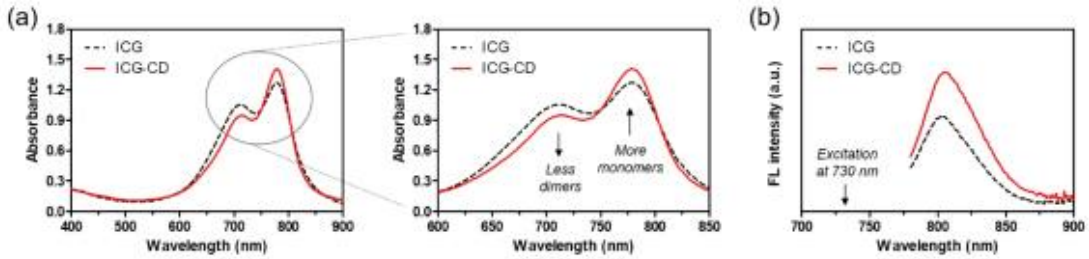

Figure 8. This figure shows the optical properties of free ICG and the ICG-CD complex. (a) Changes in the absorbance spectra of the ICG and ICG-CD solutions under the same ICG concentration. Amplification of the 710 nm and 780 nm regions show a change in absorbance of ICG-dimeric and ICG-monomeric forms in PBS. (b) Fluorescence spectra of ICG and ICG-CD solutions upon excitation at 730 nm. Absorbance and fluorescence emission spectra of each sample were obtained at a fixed ICG concentration of 10 μM in PBS at pH 7.4.

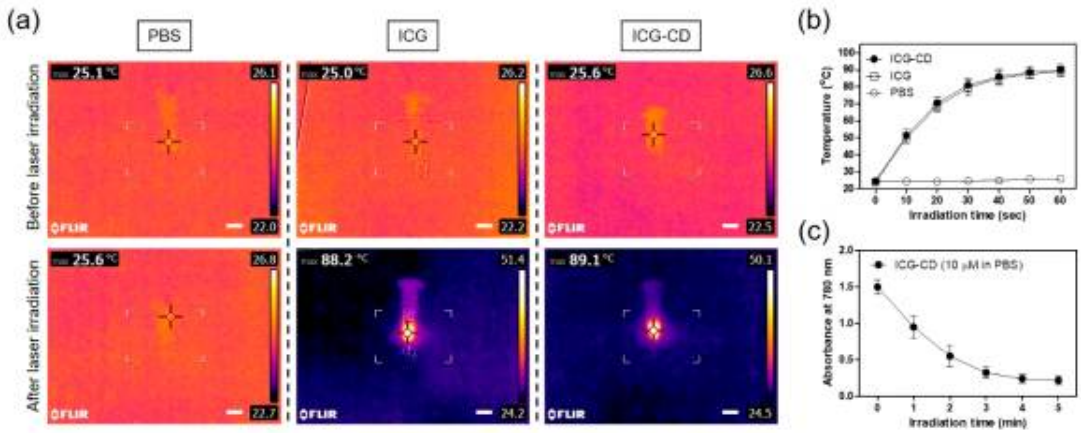

Figure 9. (a) In vitro photothermal images of the free ICG and ICG-CD complex diluted in PBS (10 nmol based on the absorbance of ICG; 100 μM is equivalent to a single dose of 0.3 mg/kg of ICG) and PBS alone (100 μL) exposed to 808 nm laser (1.1 W/cm²) for 1 min. The maximum temperature was recorded automatically via an infrared thermal camera as a function of irradiation time. Each scale bar represents 1 centimeter. **(b)** During one minute of laser irradiation, temperature changes were monitored for the solutions in each sample. **(c)** During five minutes of laser irradiation, changes in absorbance of the ICG-CD complex solution (10 μM) were measured at 780 nm. Data are expressed as the mean ± S.D. of three independent experiments.

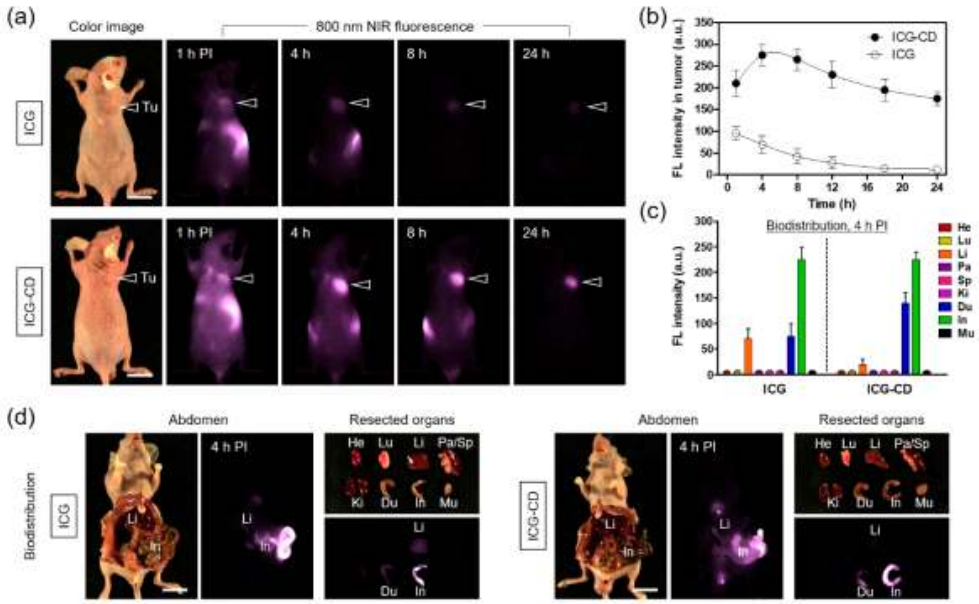

Figure 10. In vivo HT-29 tumor targeting efficiency of free ICG and the ICG-CD complex. **(a)** Reflects NIR fluorescence imaging for twenty four hours post-injection of ICG and the ICG-CD complex. **(b)** Time-dependent fluorescence intensity at tumor sites targeted by ICG and the ICG-CD complex. **(c)** Quantitative fluorescence analysis of intraoperative dissected organs at four hours post-injection of ICG and the ICG-CD complex. **(d)** This figure shows the imaging of the abdominal exploration and resected organs at four hours post-injection of ICG and the ICG-CD complex. Tumor mice were intravenously injected with 10 nmol of ICG or the ICG-CD complex and were imaged for twenty four hours. The tumor site is indicated by an arrowhead. Abbreviations include: Du, duodenum; He, heart; In, intestine; Ki, kidneys; Li, liver; Lu, lungs; Mu, muscle; Pa, pancreas; Sp, spleen; Tu, tumor; and PI, post-injection. Each scale bar represents 1 centimeter. The images are representative of three independent experiments and all NIR fluorescence images have identical exposure and normalization. The data is expressed as the mean ± S.D. of the three independent experiments.

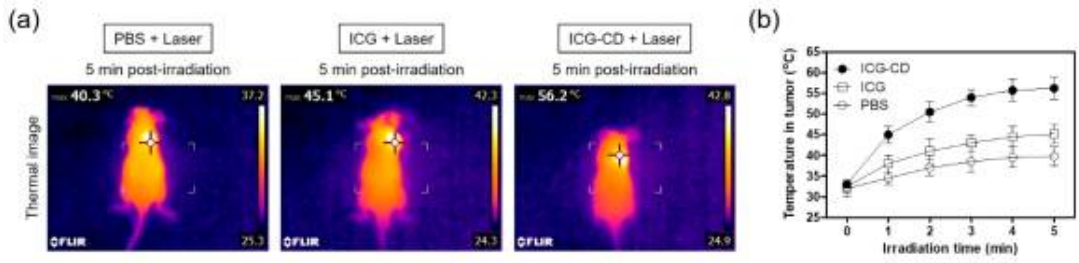

Figure 11. (a) These images reflect whole-body thermal imaging at four hours post-injection of PBS, ICG, and the ICG-CD complex of tumor-bearing mice that were exposed to five minutes of 808 nm laser irradiation (1.1 W/cm²). The maximum tumor temperatures were recorded as a function of irradiation time automatically with an infrared thermal camera. **(b)** Temperature changes at the tumor sites in each treatment group were monitored during five minutes of 808 nm laser irradiation. Data are expressed as the mean ± S.D. of three independent experiments.

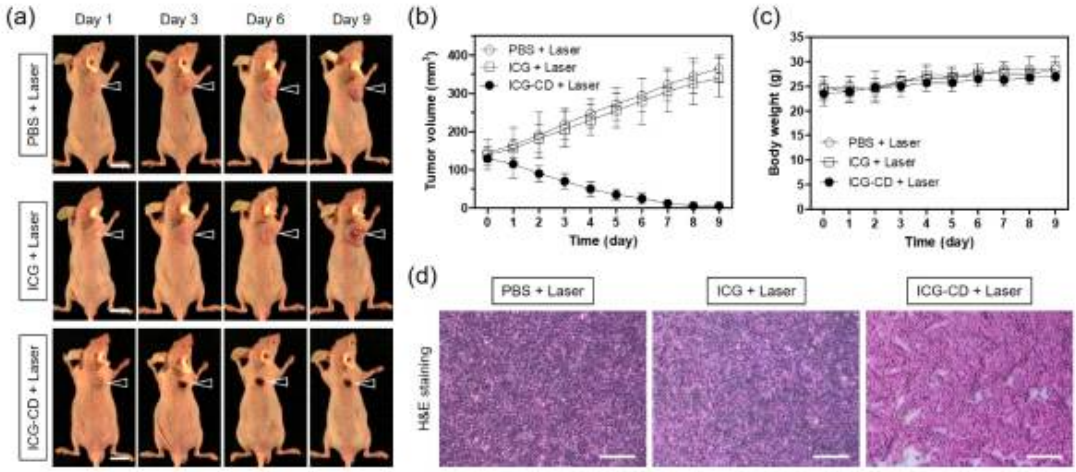

Figure 12. (a) Images are of in vivo NIR phototherapeutic efficacy. Representative images show changes in tumor size four hours post-injection of PBS, ICG, and the ICG-CD complex following a five minute 808 nm laser irradiation (1.1 W/cm^2). The tumor site is indicated by an arrowhead and each scale bar represents one centimeter. **(b)** The tumor growth rate and **(c)** body weight of each treatment group were monitored for nine days. Data are expressed as the mean ± S.D. of three independent experiments. **(d)** Tumor sections from each group were stained with H&E twenty four hours after laser irradiation. Each scale bar represents 100 μm.